ADVANCED ELECTRONIC MATERIALS
www.advelectronicmat.de

Electronic Synaptic Devices with High Thermostability Induced by Embedded Tungsten Disulfide Quantum Dots for Machine Learning

*Haoqun An, Jun Seop An, Mingjun Li, Youngjin Kim, and Tae Whan Kim**

If the speed of machine learning is to be improved, devices and systems with strong resistances to various types of internal noise, mainly internal thermal noise, are urgently needed. The successful demonstration of a synaptic device is reported based on a polyimide–tungsten disulfide quantum dot (PI-WS_2 QD) nanocomposite that continued to operate normally after simultaneous exposure of a high temperature of 100 °C. Such excellent performance is attributable to the strong quantum confinement effect of WS_2 QDs. The working current of the device and its power consumption are on the orders of nanoamperes and femtojoules, respectively. Undoubtedly, such devices will significantly improve the physical performances of machine learning systems and allow the rapid realization of greatly improving machine learning speed.

1. Introduction

The development of machine learning has expanded the scope of artificial intelligence, in areas such as driverless cars, image recognition and classification, machine translation, target recognition, even emotion recognition, and art creation, and so on. Machine learning has attracted more and more attention because it disassembles the tasks performed, which makes various types of machine assistance possible.[1–3] The process of machine learning refers to the characteristic synthesis of all kinds of similar information received by a system. This process is called "modeling". The external factors affecting the modeling speed mainly include incorrect selection of samples and the use of models that are too complex. However, compared with these, the most disturbing factors are random types of internal noise interference, such as electrical noise and internal heat generated during the device's operation.[4–6]

Improvements in artificial neural network (ANN) theory have greatly promoted the development of machine learning technology.[7–9] Even though the resistances of synaptic devices often change with the signal inputs, the changed resistances can be maintained.[10–22] Such resistance variability is very similar to the plasticity of the synaptic weight, so the synaptic devices are gradually beginning to be used as the basic units of ANN systems.[11–24] **Table 1** compares the basic performance of several typical two-terminal synaptic devices.

Electrical noise can often be solved by optimizing the hardware structure of the systems.[4] However, the internal heat generated by the current during the operation of the system is unavoidable.[4–6] For machine learning, the most direct impact of that heat is to destroy the stored content in the synaptic devices, that is, to delete part or all of the learning results, so that the system is unable to quickly match received information with similar information that had been previously received.[4,6,7,9] This leads to the fact that machines have to input a large number of samples to complete the modeling, which greatly reduces the learning speed of the machines.[4,6,7,9] The average temperature produced by electronic chips during operation is ≈70–80 °C.[25] Such a temperature environment would undoubtedly be fatal to synaptic devices driven by ion movement and filament growth. The ions and the particles that make up the filaments will diffuse, thus destroying the stored information (some even diffuse at room temperature).[14,26–28] Therefore, if the learning speeds of ANN systems are to be improved, an urgent task would be to strengthen the thermostability of synaptic devices.

This work introduces a flexible synaptic device with excellent thermostability-based on a polyimide–tungsten quantum dot (PI-WS_2 QD) nanocomposite. The resistance of the device is adjusted by the capture and release of carriers by traps in the active layer. The high thermostability of the device is attributed to the doping with WS_2 QDs. The specific electrical characteristics of the device are described, and the conduction mechanism is explained by fitting the electrical characteristic curves.

2. Results and Discussion

A schematic for the synthesis of WS_2 QDs is shown in **Figure 1**a. During the ultrasonic treatment, the WS_2 bulk is gradually exfoliated to form WS_2 nanosheets by using *N*,*N*-dimethylformamide (DMF) catalysis.[29–31] Transmission

H. An, J. S. An, M. Li, Y. Kim, T. W. Kim
Department of Electronics and Computer Engineering
Hanyang University
Seoul 04763, Republic of Korea
E-mail: twk@hanyang.ac.kr

The ORCID identification number(s) for the author(s) of this article can be found under https://doi.org/10.1002/aelm.202200876.

DOI: 10.1002/aelm.202200876

Table 1. Comparisons of data on our devices to previously reported data.

Device structure	Operation type	Operation voltage [V]	Power consumption order	High temperature resistance or not	Retention time [s]	Ref.
Al/GQD-PEDOT:PSS/ITO	Charge trapping	3	10^{-3}	No	10^{2}	[11]
Al/Cu^{2+}-PMSSQ/Al	Ion migration	3	10^{-9}	No	10^{2}	[14]
Al/PMMA-CdSe/CdZnS QD/PEDOT:PSS/ITO	Charge trapping	3	10^{-6}	No	10^{4}	[15]
Al/CEA:GQD/ITO	Charge trapping	3	10^{-6}	No	10^{4}	[16]
Ag/ZIF 8-PVP/ITO	Conduction filaments	0.8	10^{-6}	No	10^{4}	[17]
Al/zein/ITO	Conduction filaments	0.4	10^{-6}	No	10^{2}	[18]
Mg/collagen/ITO	Charge trapping	3	10^{-8}	No	–	[20]
Au/Ti_3C_2-Ag NP/ITO	Conduction filaments	2.5	10^{-3}	No	10^{3}	[23]
Ag/Melanin/ITO	Conduction filaments	1.2	10^{-3}	No	450	[24]
Al/PVA-IMGQD/ITO	Charge trapping	1.5	10^{-11}	Yes	3×10^{4}	This work

The full names of CEA-GQD and ZIF 8-PVP are chicken egg albumen-graphene quantum dot and zeolitic imidazolate framework-8-polyvinylpyrrolidone, respectively.

electron microscopy (TEM) and electron diffraction (ED) images of the WS_2 nanosheets are shown in Figure S1, Supporting Information. When the temperature in the oven reaches the boiling point of DMF (153 °C), a high pressure is formed due to the boiling of DMF in the autoclave.[29–31] In this high-temperature and high-pressure environment, DMF promotes the fracture of W=S bonds, which breaks the WS_2 nanosheets into nano-sized quantum dots.[31]

Figure 1b shows the dispersion of WS_2 QD, as well as TEM images, and the lattice spacing is 0.024 nm. The average sizes of WS_2 QDs are ≈1 to 5 nm, as shown in Figure 1c. A comparison of the X-ray diffraction (XRD) patterns for the WS_2 bulk and the WS_2 QD is shown in Figure 1d. According to existing relevant research, for WS_2 in a single-layer quantum dot state, the (002) peak should not be observed. Therefore, the XRD pattern for WS_2 QD, as shown in the figure, clearly indicates that WS_2 QDs have been successfully synthesized.[29] Figures 1e and 1f show a schematic, and the physical and cross sectional scanning electron microscope (SEM) images of the device, respectively. The average thickness of the device's active layer is seen to be ≈20 nm and that layer can be easily bent. The atomic force microscope (AFM) image shown in Figure S2, Supporting Information, indicates that the WS_2 QDs are evenly distributed in the PI matrix. The average surface roughness of the active layer was 0.17 nm. All results indicate that a PI-WS_2 QD nanocomposite can be deposited smoothly and uniformly by using a simple spin-coating process. At the same time, they also indicate that our devices can be mass-produced using a spin-coating process".[14]

Figure 2a compares the *I–V* curves for the Al/PI-WS_2 QD/ITO and the Al/PI/ITO devices (for an applied voltage from 0 to 5 V). Figure S3, Supporting Information, shows the distribution of the set voltage during 200 repetitions. As can be seen from the figure, the average set voltage value of the device is ≈4 V. Because electrons cannot tunnel through a thickness of 20 nm, no tunneling current is observed for the pure PI-based device.[32–34] However, due to the incorporation of the WS_2 QDs, the potential barrier between the two electrodes becomes significantly thinner, resulting in a tunneling current.[10,29,35,36] This is further confirmed by the curve shown in Figure S4, Supporting Information. With increasing WS_2 QD concentration, the current increased significantly. Figure 2b,c uses potential barrier diagrams to illustrate this principle. Figure S5, Supporting Information, compares the *I–V* characteristics of 25 different devices. Due to the uniform distribution of the WS_2 QDs in the PI matrix, the electrical characteristics of each device are consistent.

As a memristor, the Al/PI-WS_2 QD/ITO device exhibits different resistance change modes for different external electrical signal input.[14,17,20,21] We tried to input a small voltage several times because we expected the WS_2 QDs to be gradually filled. During 30 cycles of a positive sweep voltage (0 V → 1.5 V → 0 V), the conductance of the device gradually increases, and when same voltage sweep is applied in reverse, the device shows the same electrical characteristics, as can be seen in Figure 2d,e. Electrons tunneling through the active layer begin to be partially captured by the traps provided by WS_2 QDs.[10,11,37,38] The resistance of the device decreases mainly because the traps in the active layer are filled. When the trap is not filled, more of the tunneling electrons will be captured by the traps. At larger currents, more electrons tunnel per unit time.[37–39] In this way, more electrons are trapped by the traps, and the reduction in the resistance becomes more obvious.[37–39] Figure S6, Supporting Information, uses energy-band diagrams to depict this phenomenon.

To explore the response of the Al/PI-WS_2 QD/ITO device to the pulse, we applied more than 250 sets of positive and negative pulses (positive pulse amplitude: 1.5 V, pulse width: 10^{-3} s, interval is 10^{-3} s; negative pulse amplitude: 5.5 V, pulse width: 10^{-3} s, interval: 10^{-3} s) (all pulse widths and intervals mentioned below use these two sets of parameters). Figure 2f shows the response of the device to the first 20 sets of the pulse. When a negative pulse voltage with an amplitude of 5.5 V is applied, the trapped electrons began to be released in large quantities, and the conductance decreases sharply. From the figure, during the first 20 cycles, the conductance of the active layer can be seen to change regularly. Moreover, in the subsequent application process, the conductance of the active layer stably changes periodically. We arranged an initial state corresponding to 0.1 V in the application process and measured the conductance at

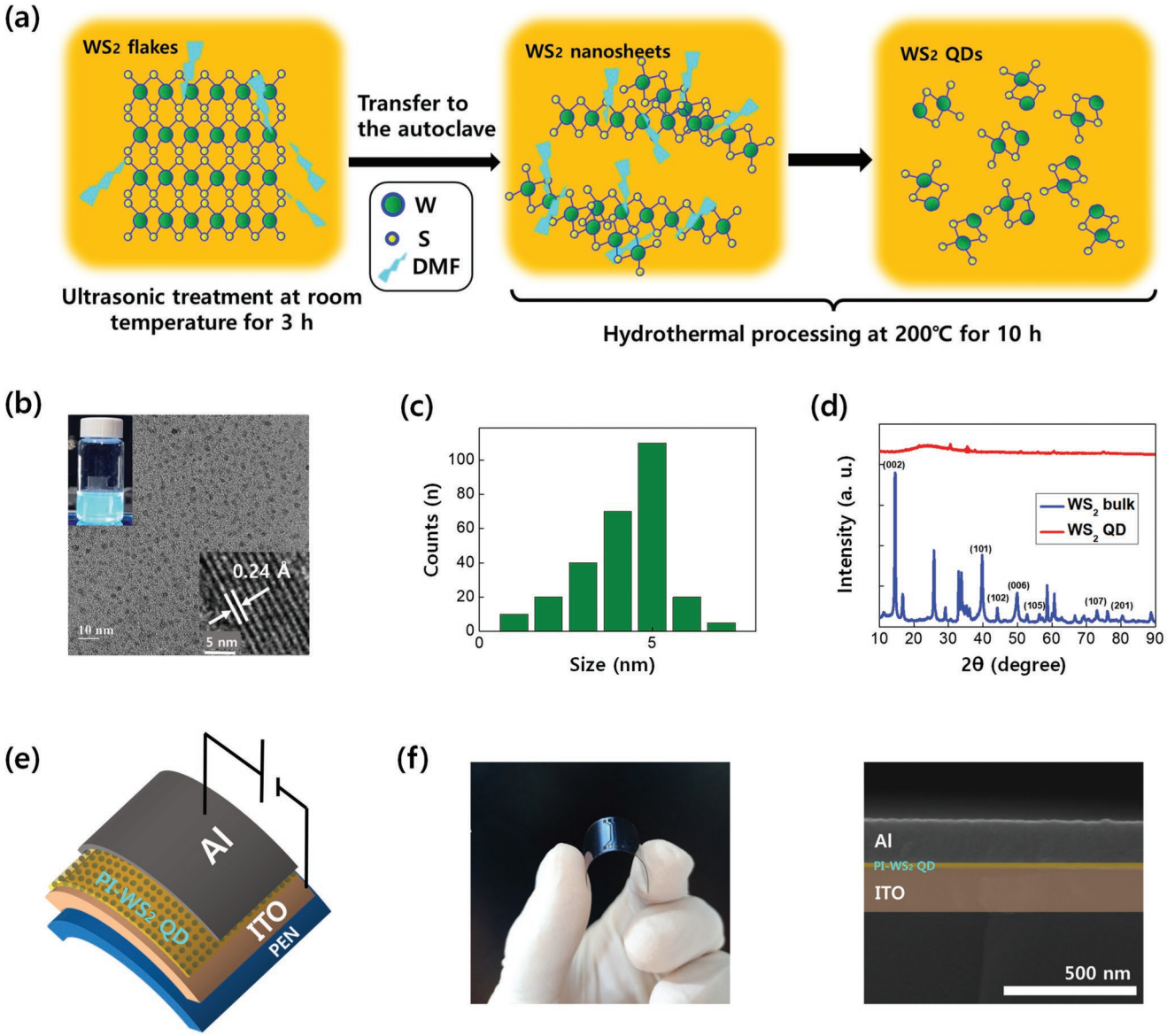

Figure 1. a) Schematic for the synthesis of WS_2 QDs. b) TEM image of WS_2 QDs (scale bars: 10 and 5 nm). c) Diameter distribution of the WS_2 QDs. d) Comparison of the XRD patterns of the WS_2 bulk and a WS_2 QD. e) Schematic and f) physical image and cross sectional image of the Al/PI-WS_2 QD/ITO synaptic device.

the 10th, 20th, and 30th applied pulse; the results are shown in Figure 2g. The conductance of the active layer corresponding to the number of applied cycles of the pulse basically maintains nearly the same value. Figure 2h records the increasing and decreasing of the conductance at the first, 20th, 50th, 100th, 150th, and 256th cycles. Figure 2i shows the electric energy consumed during the first set of positive pulse application, where the electric energy is given by $W = V \times I \times dt$, with "dt" being the pulse width.[14] The energy consumed by the device during the application of one cycle of the pulse is seen to be very low, on an order of femtojoules (fJ). It is worthy to note that with changing WS_2 QD concentration, the magnitude of the current generally changes significantly. From this point of view, reducing the WS_2 QD concentration will greatly help reduce the power consumption of the device.[14] Moreover, as Figure S7, Supporting Information, shows, the device maintains its original electrical characteristics, after having been exposed to air for more than 3 months and after having been repeatedly bent for 1×10^4 times. Due to its good anti-fatigue properties, PI will not be structurally damaged, not even after having been repeatedly bent for more than 1×10^4 times. In addition, without the application of a strong external electric field, the electrons captured in the WS_2 QDs cannot be released, so the resistance of the active layer will not change.[32–34,37,38]

Whether the trapped electrons can be firmly bound in the traps of the active layer is the key to data storage. **Figure 3**a compares the *I–V* characteristic curves for the Al/PI-WS_2 QD/ITO and the Al/PI-WS_2 NS/ITO devices exposed to 100 °C (for an applied voltage from 0 to 5 V). The $\log(I/V^2)$–$1/V$ fitted curves shown in Figure S8a,b, Supporting Information, indicate that

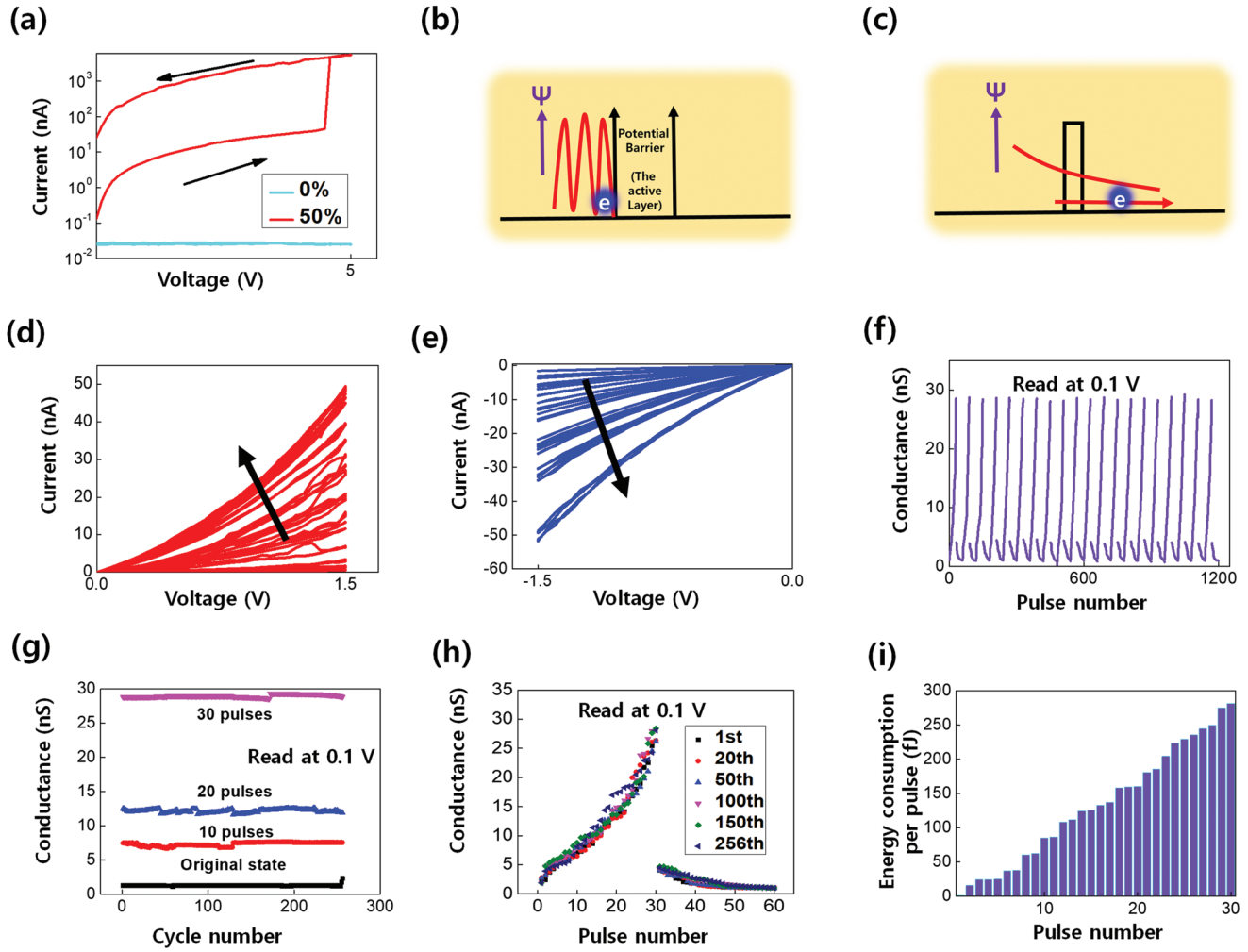

Figure 2. a) Comparison at an applied voltage of 0 →5 → 0 V between the *I–V* curve for the PI-WS_2 QD nanocomposite with a WS_2 QD concentration of 50% and the *I–V* curve for a pure PI- based devices. b,c) Potential barrier diagrams of a pure PI active layer (b) and the PI-WS_2 QD nanocomposite (c) with a 50% concentration of WS_2 QD. d,e) *I–V* curves of an Al/PI-WS_2 QD/ITO synaptic device driven by positive (d) and negative (e) voltage sweeps. f) Variation in the conductance of an Al/PI-WS_2 QD/ITO synaptic device driven by positive (1.5 V, 10^{-3} s) and negative electric pulse (–5.5 V, 10^{-3} s) of the first 20 cycles. g) Conductance distributions for resistance states in 256 cycles of pulse applications. h) Conductance variations in the first, 20th, 50th, 100th, 150th, and 256th cycles of pulse applications. i) Distribution of the electric energy consumed during the first cycle of the positive pulse.

for the two devices, the hot electrons emitted from the ITO electrode flow through the active layer by direct tunneling in the lower voltage range. For the tunneling electrons, the relationship between the current and the barrier thickness can be described as follows:[40–42]

$$J \approx exp\left(-\frac{4\pi L}{h}\sqrt{2q\phi_B m}\right) \quad (1)$$

where $q\phi_B$ is the Schottky barrier, L the thickness of barrier, m the effective mass of electron, and h Planck's constant.[41,42] Because WS_2 NSs contain more trap centers than WS_2 QDs, the barrier of the active layer of the Al/PI-WS_2 NS/ITO device is thinner as shown in Figure S8c,d, Supporting Information.[43] In this way, the number of electrons tunneling through the active layer of the Al/PI-WS_2 NS/ITO device is larger at the same voltage.[41–43]

Then we fitted the section in the *I–V* curve form of 2.5 to 4.1 V for the Al/PI-WS_2 NS/ITO device and found that log (I/V) versus $V^{1/2}$ plot showed a highly linear relationship, as shown in Figure 3b. This indicates that in this voltage range, the conduction mechanism of the device conforms to hopping conduction.[44,45] In other words, a considerable part of the trapped electrons obtain enough energy due to heating and tunnel between the WS_2 NSs separated by the barriers. When the potential barriers become thinner due to an applied electric field, the wave function of the electrons in each trap can be extended to cover other traps.[36,43] Therefore, when the applied voltage increases to a sufficient value, a directional hopping current will naturally form.[36,43] However, for the Al/PI-WS_2 QD/ITO device, there is no hopping current because the barriers between WS_2 ODs are too thick. A schematic for this process is shown in Figure S9, Supporting Information. For the interval from 4.2 to 5 V, the log(I/V^2) versus $1/V$ fit to the *I–V* curve

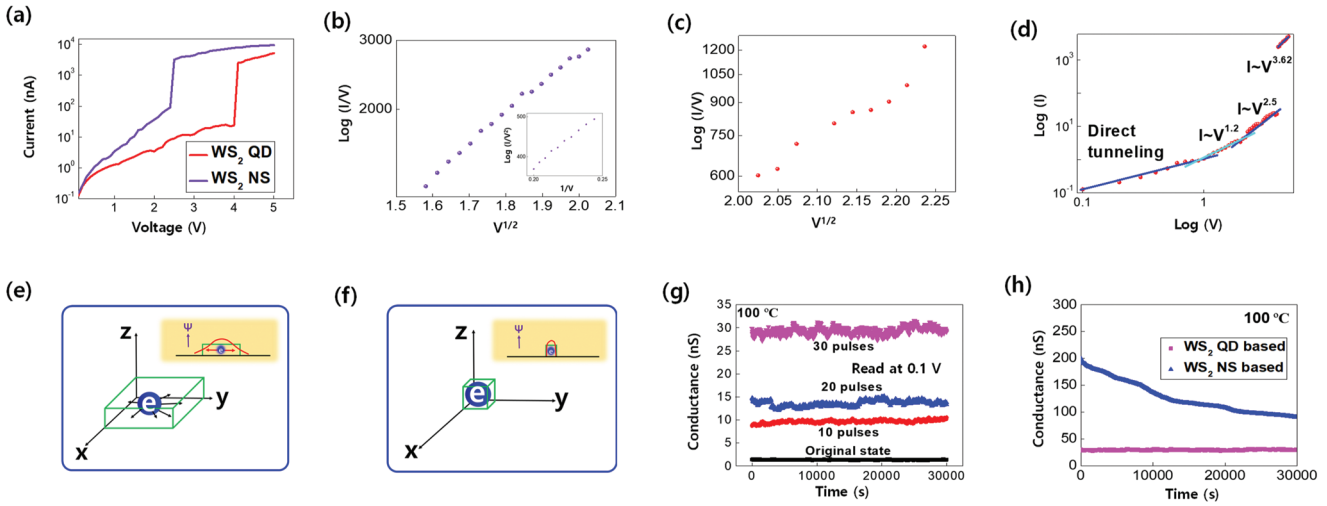

Figure 3. a) Comparison of the *I–V* curves for the Al/PI-WS_2 QD/ITO and the Al/PI-WS_2 NS/ITO devices under a varying applied voltage from 0 to 5 V. b) The $\log(I/V)$–$V^{1/2}$ fitting result for the interval from 2.5 to 4.1 V in the *I–V* curve for the Al/PI-WS_2 NS/ITO device, and the insert exhibits the $\log(I/V^2)$–$1/V$ fitting result for the interval from 4.2 to 5 V in the *I–V* curve for the Al/PI-WS_2 NS/ITO device. c) The $\log(I/V)$–$V^{1/2}$ fitting result for the interval from 4 to 5 V in the *I–V* curve for the Al/PI-WS_2 QD/ITO device. d) The log–log fitted *I–V* curves for an Al/PI-WS_2 QD/ITO device in the interval from 0 to 5 V. In the voltage range from 1 to 2 V, the slope of the *I–V* curve was 1.2 indicative of a small number of electrons being trapped by the WS_2 QDs. When the voltage exceeds 2 V, a large number of electrons begin to be trapped by the WS_2 QDs, the slope is 2.5, which indicate that the conduction mechanism conforms to space charge limited conduction. All the WS_2 QDs are filled with electrons and the device transition to a low resistance state, while the voltage reaches 4 V. e,f) Schematic and wave function diagrams of electron binding in the WS_2 NS (e) and the WS_2 QD (f). g) Maintenance time of the conductance in each state at 100 °C. h) Comparison of conductance maintenance times for PI-WS_2 QD-based and PI-WS_2 NS-based devices at 100 °C (after 30 pulses had been applied). The concentrations of the WS_2 QDs and the WS_2 NSs were 50%.

is linear (as shown in the insert of Figure 3b), indicating that the conduction of the device is governed by the direct tunneling mechanism.[41,42] When the voltage is sufficiently large (more than 4.2 V), the barriers between the traps are too thin to bind the electrons, so all the injected electrons can tunnel through the active layer.[44,45] In this process, the injected electrons are in a trap-free state.[44,45] Figure 3c shows the $\log(I/V)$–$V^{1/2}$ fitted *I–V* curve from 4 to 5 V for the Al/PI-WS_2 QD/ITO device. From the figure, the $\log(I/V)$ versus $V^{1/2}$ plot can be seen to not be linear. This indicates that no tunneling electron manifold exists between WS_2 QDs.[44,45] As shown in Figure 3d, the slope of the log–log fitting line is 3.62, indicating that the electrons trapped by the WS_2 QDs are still firmly bound, although the Al/PI-WS_2 QD/ITO device is exposed to a high temperature of 100 °C, and that the main component of the current is due to electrons tunneling between the two electrodes.[10,38] The reason for all the phenomena above is most likely because the electrons trapped by the WS_2 NSs have freedom in the "x" and the "y" directions, while the motion of the electrons trapped by the WS_2 QDs are limited in all directions. This is the so-called quantum confinement effect, as shown in Figure 3e,f.[36,43]

Figure 3g shows the retention curves for the initial state and for the state after having applied a 1.5 V pulse for 10, 20 and 30 times to the Al/PI-WS_2 QD/ITO device, at a temperature of 100 °C. During the test time of 3×10^4 s, no significant change was found in the conductance of the Al/PI-WS_2 QD/ITO device. The electrons captured by the WS_2 QDs were still firmly bound, even though the temperature was 100 °C. The strong binding force of the WS_2 QDs on the electrons is due to their strong quantum confinement effect.[43] As a comparative experiment, we also measured the retention of an Al/PI-WS_2 NS/ITO device. After having applied 30 pulses with an amplitude of 0.7 V to the Al/PI-WS_2 NS/ITO device, we placed it in a high-temperature environment of 100 °C. The electrons that gain energy because of the heating gradually become unbound, so that the conductance continues to decrease, as shown in Figure 3h.

Figure 4a–d shows the hysteresis characteristics and endurance of an Al/PI-WS_2 QD/ITO device in a 100 °C environment. It can be seen from the figures that the electrical characteristics of Al/PI-WS_2 QD/ITO devices remain basically stable even under the environment of 100 °C, which indicate that the binding force of WS_2 QDs on electrons makes it impossible for electrons to escape to form thermal current. Moreover, even if the device is placed in a 100 °C environment for a period of time, its various resistance states will not change easily. Figure S10, Supporting Information, exhibits the differential scanning calorimetry (DSC) curve for the PI-WS_2 QD nanocomposite. It can be seen from the figure that the glass transition temperature of the PI-WS_2 QD nanocomposite is 170 °C, which indicates that the state of the active layer does not change at 100 °C.

A 5 by 5 array composed of Al/PI-WS_2 QD/ITO devices with polyethylene naphthalate (PEN) as the substrate was repeatedly bent for more than 1×10^4 times and placed in an environment at a temperature of 100 °C. Pulses with amplitudes of 1.5 V were applied to the ports corresponding to the device in the yellow area in Figure 4e, which briefly depicts the layout of the experiment. After 1.5 V pulse has been applied 30 times, the letter "H" can be clearly seen in the array, and the array completes the preliminary learning of the information, as shown in Figure 4f. This is completely consistent with the operation of the device at room temperature, as shown in Figure 4g,h. Moreover, the

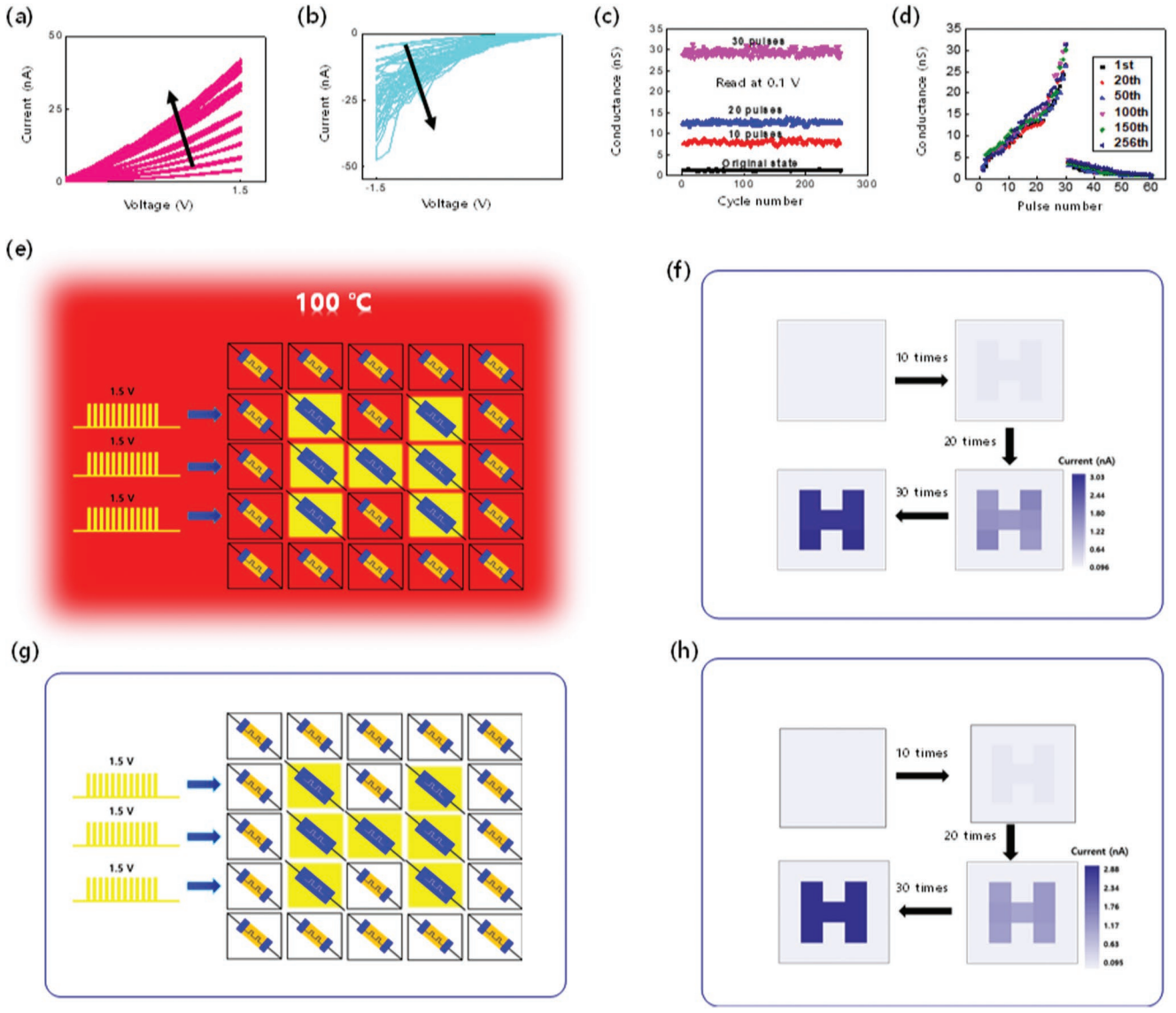

Figure 4. a,b) *I–V* curves for the Al/PI-WS_2 QD/ITO synaptic device driven by a positive (a) and a negative (b) sweeping voltage at 100 °C. c) Conductance distribution of each resistance state in 256 cycles of pulse applications at 100 °C. d) Conductance variations in the first, 20th, 50th, 100th, 150th, and 256th cycles of pulse applications at 100 °C. e) Schematic for the method used for the anti-noise interference test at a high temperature of 100 °C. Input pulse signal for the learning content (1.5 V, 10^{-3} s) to the "H" area in a 5 by 5 array at the same time. f) Schematic for the learning process. g) Schematic for the machine learning process at room temperature. The input pulse signal for the learning content (1.5 V, 10^{-3} s) to the "H" area in a 5 by 5 array at the same time. h) Schematic for the learning process at room temperature. The reading voltage of all electrodes was 0.1 V.

learning results at each stage will not destroyed by the high temperature, as shown in Figure S11, Supporting Information. Even when the temperature rises to 150 °C, the device still operates normally. Figure S12, Supporting Information, shows that the information stored in the device can be maintained for more than 10^5 s even in an environment with a temperature of 150 °C. However, when the temperature rises to 155 °C, forgetting begins to occur. When the temperature exceeds 150 °C, the trapped electrons obtain enough energy to break free from the WS_2 QDs. Figure S13, Supporting Information, exhibits the learning process of the device in an environment with a temperature of 150 °C. Until the temperature reaches 150 °C, the device still performs normal learning. However, for Al/PI-WS_2 NS/ITO devices, due to the relatively weak binding force of the WS_2 NSs on the electrons, the learning results are gradually destroyed at 5×10^3 s, as shown in Figure S14, Supporting Information.

To evaluate the recognition capability of the Al/PI-WS_2 QD/ITO synaptic devices, we used a Modified National Institute of Standards and Technology (MNIST) method to conduct pattern recognition simulations on the data shown in Figure 4a. The main information obtained from the Modified National Institute of Standards and Technology (MNIST) simulation and learning algorithm is shown in Figure S15, Supporting Information, and the pattern recognition process is shown in **Figure 5**a. The input of the system is determined by 784 (28 × 28) pixels

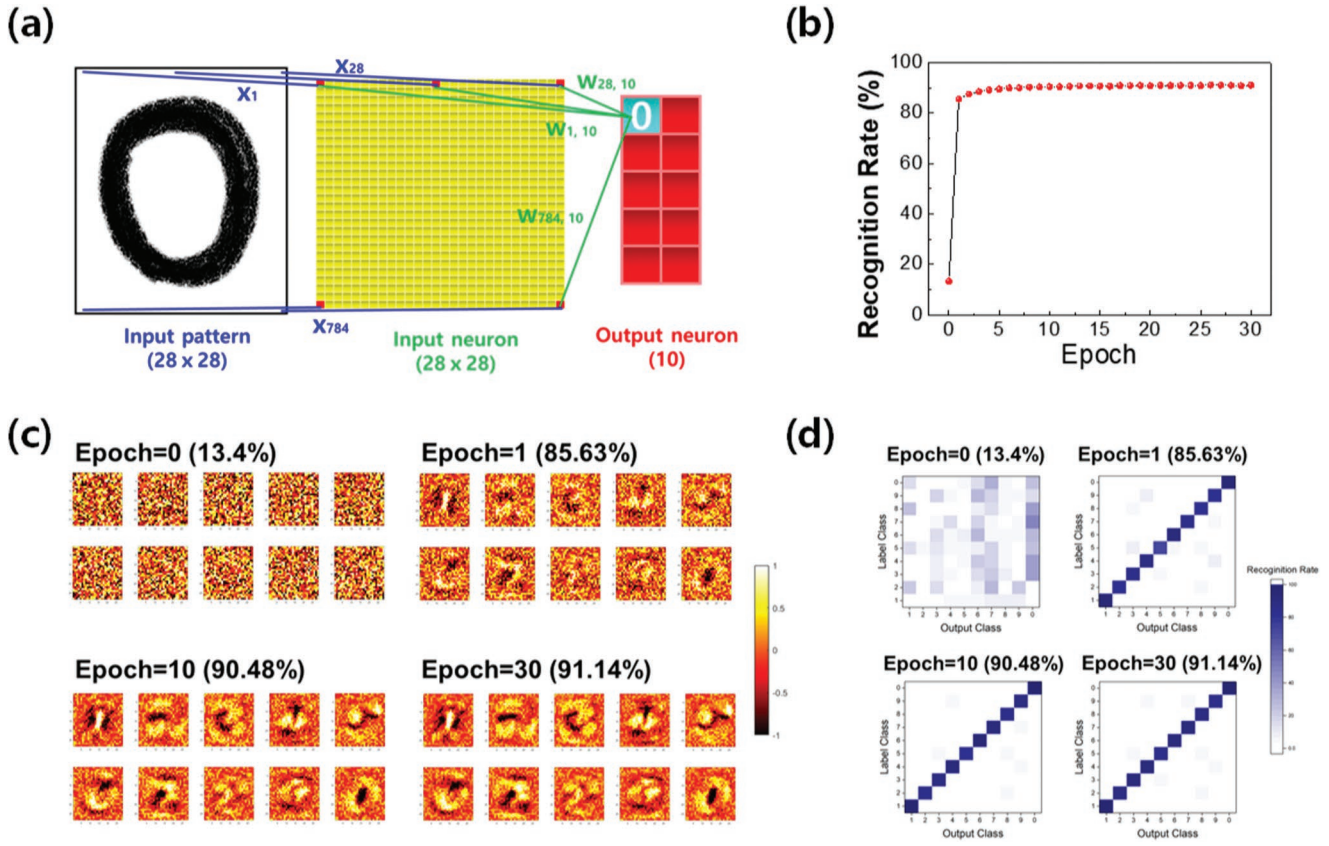

Figure 5. a) Schematic for a single layer network for recognition of the number "0". The input pattern "0" (28 × 28), input neurons (28 × 28, yellow), and output neurons (2 × 5, red) are fully connected. b) Relationship between learning times and the recognition rate. c) Weight value and d) heap maps of the device's learning process for numbers from 0 to 9 at a temperature of 100 °C.

and 784 neurons, and the output consists of 10 (2 × 5) neurons. The synaptic weights of the 784 neurons are variable, and the 10 output units correspond to the numbers from "0" to "9". As shown in Figure 5b, without any learning, the initial recognition rate of the device is 13.4%. After 60 000 times of learning about each number, we tested the device 10 000 times with the same number. The recognition rate means that the ratio of the device to recognize these numbers is 85.63%. The weight value map and the heap map for this process are shown in Figures 5c and 5d, respectively. With increasing training times, the memory of the numbers by the devices gradually becomes clearer and more specific, and the tiles in the confusion matrix become arranged diagonally and have the largest saturated color. All these indicate that the Al/PI-WS_2 QD/ITO synaptic device can correctly infer each number through training.[18]

3. Conclusion

In an Al/PI-WS_2 QD/ITO synaptic device, the conductance of active layer undergoes a rapid change due to the trapping of electrons emitted from the electrodes. Even at a high temperature of 100 °C, the device continued to operate normally, and the learning results at each stage were maintained, which should greatly improve the efficiency of modeling, and significantly improve the speed of machine learning. Such excellent performance is attributable to the strong quantum confinement effect of the WS_2 QDs, as a 2D material, on the trapped electrons. We believe that these experimental results provide important information for future research on high thermostability synaptic devices whose "conduction mechanism depends on defects in insulating active layer" and on other types of devices with the similar functions.

4. Experimental Section

Synthesis of the PI-WS_2 QD Nanocomposite: WS_2 QDs were synthesized by using the hydrothermal method. The WS_2 bulk (250 mg) was put into 5 mL of DMF. After ultrasonic treatment for 3 h, a transparent dark green WS_2 nanosheet (NS) dispersion was obtained. The obtained WS_2 NSs dispersion was then put into an autoclave and treated in vacuum at 200 °C for 10 h. The obtained transparent light green clear liquid was a dispersion of WS_2 QDs. The obtained WS_2 QD dispersion was mixed into a PI/DMF dispersion with a PI concentration of 50 mg mL^{-1}, and stirred for 3 h to obtain a PI-WS_2 QD mixture.

Fabrication of the Al/PI-WS_2 QD/ITO Synaptic Device: A spin coating method (rotating speed: 1000 rpm for 10 s → 3000 rpm for 20 s → 5000 rpm for 30 s → 3000 rpm for 20 s → 1000 rpm for 10 s) was used to coat the prepared PI-WS_2 QD mixture on the surface of an ITO electrode that had been treated with ultraviolet light, after which the ITO electrode coated with a PI-WS_2 QD nanocomposite was annealed on a hot plate at 150 °C for 3 h. Finally, to complete the preparation of the device, the thermal evaporation method was used in a vacuum of 1 × 10^{-6} Torr, to deposit Al electrode with a thickness of 200 nm.

Characterization: All electrical characteristics of the device were measured by using a Keithley 4200. TEM images were obtained by using a CM30 TEM system at a driving voltage of 300 kV. SEM images were acquired out by using a Nova Nano SEM 450 system, and XRD patterns for the WS_2 bulk and the WS_2 QD were measured with the help of a SmartLab instrument, UPS spectra was determined with the aid of a theta probe base system (Thermo Fisher Scientific). The data for the differential scanning calorimetry (DSC) curve were carried out by a SDT Q600, Auto-DSCQ20 System. AFM images were carried out by using a Dimension 3100 (Vecco, CA) system in the tapping mode.

Supporting Information

Supporting Information is available from the Wiley Online Library or from the author.

Acknowledgements

This research was supported by the National Research Foundation of Korea (NRF) grant funded by the Korea government (MSIT) (No. 2022R1I1A4053429) and the National Research Foundation of Korea (NRF) grant funded by the Korea government (MSIT) (No. 2018R1A5A7025522).

Conflict of Interest

The authors declare no conflict of interest.

Data Availability Statement

The data that support the findings of this study are available from the corresponding author upon reasonable request.

Keywords

high thermal stability, quantum confinement effect, synaptic devices, tunneling current, WS_2 quantum dots

Received: August 3, 2022
Revised: October 19, 2022
Published online:

[1] M. I. Jordan, T. M. Mitchell, *Science* **2015**, *349*, 255.
[2] G. Carleo, I. Cirac, K. Cranmer, L. Daudet, M. Schuld, N. Tishby, L. Vogt-Maranto, L. Zdeborová, *Rev. Mod. Phys.* **2019**, *91*, 045002.
[3] K. G. Liakos, P. Busato, D. Moshou, S. Pearson, D. Bochtis, *Sensors* **2018**, *18*, 2674.
[4] D. M. Hawkins, *J. Chem. Inf. Comput. Sci.* **2004**, *44*, 1.
[5] R. Biswas, L. Blackburn, J. Cao, R. Essick, K. A. Hodge, E. Katsavounidis, K. Kim, Y.-M. Kim, E.-O. L. Bigot, C.-H. Lee, J. J. Oh, S. H. Oh, E. J. Son, Y. Tao, R. Vaulin, X. Wang, *Phys. Rev. D* **2013**, *88*, 062003.
[6] G. Vajente, Y. Huang, M. Isi, J.C. Driggers, J.S. Kissel, M.J. Szczepańczyk, S. Vitale, *Phys. Rev. D* **2020**, *101*, 042003.
[7] W. Samek, A. Binder, G. Montavon, S. Lapuschkin, K.-R. Müller, *IEEE Trans. Neural Networks Learn. Syst.* **2016**, *28*, 2660.
[8] T. Bouwmans, S. Javed, M. Sultana, S. K. Jung, *Neural Networks* **2019**, *117*, 8.
[9] J. Mehrer, C. J. Spoerer, N. Kriegeskorte, T. C. Kietzmann, *Nat. Commun.* **2018**, *11*, 5725.
[10] H. An, Y. Kim, M. Li, T. W. Kim, *Small* **2021**, *17*, 2102772.
[11] J. Hur, B. C. Jang, J. Park, D.-I. Moon, H. Bae, J.-Y. Park, G.-H. Kim, S.-B. Jeon, M. Seo, S. Kim, S.-Y. Choi, Y.-K. Choi, *Adv. Funct. Mater.* **2018**, *28*, 1804844.
[12] F. Guo, M. Song, M.-C. Wong, R. Ding, W. F. Io, S.-Y. Pang, W. Jie, J. Hao, *Adv. Funct. Mater.* **2022**, *32*, 2108014.
[13] D.-G. Seo, Y. Lee, G.-T. Go, M. Pei, S. Jung, Y. H. Jeong, W. Lee, H.-L. Park, S.-W. Kim, H. Yang, C. Yang, T.-W. Lee, *Nano Energy* **2019**, *65*, 104035.
[14] C. Wu, T. W. Kim, H. Y. Choi, D. B. Strukov, J. J. Yang, *Nat. Commun.* **2017**, *8*, 752.
[15] B. M. Koo, S. Sung, C. Wu, J.-W. Song, T. W. Kim, *Sci. Rep.* **2019**, *9*, 9755.
[16] S. Sung, J. H. Park, C. Wu, T. W. Kim, *Sci. Rep.* **2020**, *10*, 1255.
[17] Y. J. Jeon, H. An, Y. Kim, Y. P. Jeon, T. W. Kim, *Appl. Surf. Sci.* **2021**, *567*, 150748.
[18] Y. Kim, C. H. Park, J. S. An, S. H. Choi, T. W. Kim, *Sci. Rep.* **2021**, *11*, 20633.
[19] S. Chen, E. Li, R. Yu, H. Yang, Y. Yan, Y. Hu, H. Chen, T. Guo, *J. Mater. Chem. C* **2021**, *9*, 9972.
[20] H. Wang, M. Yang, Q. Tang, X. Zhao, Y. Tong, Y. Liu, *Adv. Funct. Mater.* **2019**, *29*, 1901107.
[21] L. Shao, Y. Zhao, Y. Liu, *Adv. Funct. Mater.* **2021**, *31*, 2101951.
[22] E. Li, X. Wu, Q. Chen, S. Wu, L. He, R. Yu, Y. Hu, H. Chen, T. Guo, *Nano Energy* **2021**, *85*, 106010.
[23] L. Guo, B. Mu, M.-Z. Li, B. Yang, R.-S. Chen, G. Ding, K. Zhou, Y. Liu, C.-C. Kuo, S.-T. Han, Y. Zhou, *ACS Appl. Mater. Interfaces* **2021**, *13*, 39595.
[24] M. Chen, Z. Lv, F. Qian, Y. Wang, X. Xing, K. Zhou, J. Wang, S. Huang, S.-T. Han, Y. Zhou, *J. Mater. Chem. C* **2021**, *9*, 3569.
[25] K. M. Chen, D. S. Jiang, N. H. Kao, J. Y. Lai, *Microelectron. Reliab.* **2006**, *46*, 155.
[26] G. J. Dienes, A. C. Damsk, *J. Appl. Phys.* **1958**, *29*, 1713.
[27] R. M. Young, R. McPherson, *J. Am. Ceram. Soc.* **1989**, *12*, 1080.
[28] B. G. Streetmen, S. K. Banerjee, *Solid State Electronic Devices*, Pearson Education, Upper Saddle River, NJ, USA **2005**.
[29] A. Bayat, E. Saievar-Iranizad, *J. Lumin.* **2017**, *185*, 236.
[30] S. Ding, N. Jiao, *Angew. Chem., Int. Ed.* **2012**, *51*, 9226.
[31] C. Wu, T. W. Kim, J. H. Park, H. An, J. Shao, X. Chen, Z. L. Wang, *ACS Nano* **2017**, *11*, 8356.
[32] D. J. Liaw, K. L. Wang, Y. C. Huang, K. R. Lee, J. Y. Lai, C. S. Ha, *Prog. Polym. Sci.* **2012**, *37*, 907.
[33] A. K. John, J. R. Edman, *Adv. Mater.* **1998**, *15*, 10.
[34] I. Gouzman, E. Grossman, R. Verker, N. Atar, A. Bolker, N. Eliaz, *Adv. Mater.* **2019**, *31*, 1807738.
[35] C. Caroli, R. Combescot, P. Nozieers, D. James-Saint, *J. Phys. C: Solid State Phys.* **1971**, *4*, 916.
[36] A. Beiser, *Concepts of Modern Physics*, McGraw-Hill, New York, NY **2003**.
[37] M. A. Lampert, *Phys. Rev.* **1956**, *103*, 1648.
[38] P. Mark, W. Helfrich, *J. Appl. Phys.* **1962**, *33*, 205.
[39] J. G. Simmons, *Phys. Rev.* **1968**, *166*, 912.
[40] E. L. Murphy, R. H. Good, Jr., *Phys. Rev.* **1956**, *102*, 1464.
[41] C. Caroli, R. Combescot, P. Nozieres, D. Saint-James, *J. Phys. C: Solid State Phys.* **1971**, *4*, 916.
[42] J. V. Morgan, E. O. Kane, *Phys. Rev. Lett.* **1959**, *3*, 466.
[43] E. A. Johnson, *Low-Dimensional Semiconductor Structure: Fundamentals and Device Applications* (Eds: K. Barnham, D. Vvedensky), The Edinburgh Building, Cambridge, UK **2001**, Ch. 2.
[44] P. C. Arnett, N. Klein, *J. Appl. Phys.* **1975**, *46*, 1399.
[45] M. Pollak, *J. Non-Cryst. Solids* **1972**, *11*, 1.